

Figure 2. Charge formation in a diatomic molecule as predicted by the techniques of Huheey (lines) and Sanderson (squares). See text.

Sanderson electronegativities with charge (hardness) is in some manner constantly proportional to the initial electronegativities. In other words, a constant value of γ is implicit in the Sanderson electronegativity values, as supported by Figure 1. However, experimental results^{11,12,16} yield values of γ that vary considerably and by an amount that would be severely detrimental to the performance of the polar covalent model, if the magnitude of the variations were manifested directly. One explanation that comes to mind to explain these discrepancies is to suggest that on an atomic ("local") scale the electronegativity and hardness are in

fact proportionally constant. However, the experimental data from which the values for Mulliken style electronegativities are derived reflect the "global" energies (ionization potential and electron affinity), which incorporate energy components that are not manifested on the local scale. Chief among the extraneous energies is the work involved in transferring the manipulated electrons to and from infinity, which may add substantial and variable contributions to the ionization and affinity energies. The size and electron density of an atom (upon which Sanderson electronegativities are based) may be more appropriate indicators of the local electronic environment. In partial confirmation of this discussion, the deviation of the Mulliken-Jaffé electronegativity values for the first-row elements from those predicted by the simple correlation (eq 10a) with the Sanderson electronegativities varies roughly in proportion to the deviation of the γ values about the norm.

Conclusion

We conclude from the agreement observed in Figure 1 that the concept of the hardness as being constantly proportional to the electronegativity (γ is constant) is implicit in the Sanderson electronegativities. Also, in accordance with Parr and Bartolotti,¹⁰ we find that the geometric mean electronegativity and hardness equilibration postulates are not appropriate for utilization in electronegativity systems described by density functional theory (eq 1). The identification of the harmonic mean as an appropriate vehicle for electronegativity equilibration leads to the application of the harmonic mean to hardness equilibration. These conclusions stem from our demonstration that applying the geometric mean to Sanderson electronegativities is functionally equivalent to applying the harmonic mean to the latter group of electronegativities.

Direct Determination of the Limiting High-Pressure Rate Constants of the System $\text{FSO}_3 + \text{FSO}_3 \rightleftharpoons \text{F}_2\text{S}_2\text{O}_6$ over the Temperature Range 293–381 K

C. J. Cobos, A. E. Croce de Cobos, H. Hippler,[†] and E. Castellano*

Instituto de Investigaciones Fisicoquímicas Teóricas y Aplicadas (INIFTA),[‡] C. C. 16, Sucursal 4, (1900) La Plata, Argentina (Received: October 19, 1987; In Final Form: June 7, 1988)

The laser flash photolysis/absorption technique has been used to measure directly the approach to equilibrium in the system $\text{FSO}_3 + \text{FSO}_3 \rightleftharpoons \text{F}_2\text{S}_2\text{O}_6$ over the temperature range 293–381 K and the pressure range 250–760 Torr of He and CF_4 . The rate constants have been found to be independent of pressure, being $k_{\text{rec},\infty} = 4.64 \times 10^{-14} (T/300)^{(0.72 \pm 0.25)} \text{ cm}^3 \text{ molecule}^{-1} \text{ s}^{-1}$ between 293 and 381 K, and $k_{\infty} = 2.09 \times 10^{14} \exp[-(11090 \pm 290)/T] \text{ s}^{-1}$ between 321 and 381 K. The pressure dependence of the equilibrium constants derived here gives a value for ΔH_{298}° of $22.1 \pm 0.7 \text{ kcal mol}^{-1}$ and for ΔS_{298}° of $38.2 \pm 1.0 \text{ cal mol}^{-1} \text{ K}^{-1}$. The errors that are quoted correspond to two standard deviations. The low $k_{\text{rec},\infty}$ obtained can be described by the canonical version of the statistical adiabatic channel model with a standard value of 0.46 for the parameter α/β .

Introduction

The recombination of radicals and the reverse simple bond dissociation reactions are fairly well-understood processes. Many experimental data of high-pressure rate constants have been recently evaluated in terms of the canonical version of the statistical adiabatic channel model (SACM).^{1,2} Most of these calculations have been performed for simple bond fission reactions of strongly bound compounds. The comparison of this theory with recombination-dissociation experiments in the case of the fission of weak bonds, still stronger than those of van der Waals molecules, appears to be of great importance. The interest arises because the sta-

tistical theories, which are based on a rapid and complete randomization of the internal energy, might not apply for van der Waals molecules. In this case the reaction could compete with intramolecular dynamics. Recently, some studies on the recombination reactions $\text{NO} + \text{NO}_2 \rightarrow \text{N}_2\text{O}_3$,^{3,4} $\text{NO}_2 + \text{NO}_2 \rightarrow \text{N}_2\text{O}_4$,⁵ and $\text{NO}_2 + \text{NO}_3 \rightarrow \text{N}_2\text{O}_5$ ⁶ have been reported. For these com-

(1) Troe, J. J. *Chem. Phys.* **1981**, *75*, 226.

(2) Cobos, C. J.; Troe, J. J. *Chem. Phys.* **1985**, *83*, 1010.

(3) Smith, I. W. M.; Yarwood, G. *Chem. Phys. Lett.* **1986**, *130*, 24.

(4) Smith, I. W. M.; Yarwood, G. *Faraday Discuss. Chem. Soc.* **1987**, *84*, 205.

(5) Borrell, P.; Cobos, C. J.; Croce de Cobos, A. E.; Hippler, H.; Luther, K.; Ravishankara, A. R.; Troe, J. *Bunsen-Ges. Phys. Chem.* **1985**, *89*, 337.

(6) Borrell, P.; Cobos, C. J.; Luther, K. *J. Phys. Chem.* **1988**, *92*, 4377.

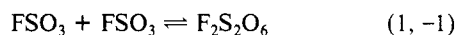
(7) Croce de Cobos, A. E.; Hippler, H.; Troe, J. J. *Phys. Chem.* **1984**, *88*, 5083.

[†] Permanent address: Institut für Physikalische Chemie der Universität Göttingen, Göttingen, West Germany.

[‡] Facultad de Ciencias Exactas, Universidad Nacional de La Plata.

pounds the N–N bond dissociation energies are 9.8, 13.6, and 22.2 kcal mol⁻¹, respectively, and the absolute values for the limiting high-pressure rate constants are close to 10⁻¹² cm³ molecule⁻¹ s⁻¹ (3.4 × 10⁻¹², 8.3 × 10⁻¹³, and 2.2 × 10⁻¹² cm³ molecule⁻¹ s⁻¹, respectively). These values are well below results from phase space theory, but still relatively loose transition states account for the observed rate constants. In all cases SACM calculations have reproduced the experimental values with the general α/β parameter being in the normal range of $\alpha/\beta = 0.46 \pm 0.09$.² Here α is the global looseness parameter of the angular potentials and β is the Morse parameter of the dissociating bond.

A low bond dissociation energy of about 22 kcal mol⁻¹ has been reported for the peroxide linkage in the peroxydisulfuryl difluoride F₂S₂O₆.^{7,8} This compound is in equilibrium at ordinary temperatures with the fluorosulfate radicals FSO₃ according to



In spite of the weakness of this O–O bond, a temperature-independent limiting high-pressure recombination rate constant of around 5.0 × 10⁻¹⁴ cm³ molecule⁻¹ s⁻¹ over the temperature range 293–323 K has been reported.⁹ This value is much lower than standard values of about 10⁻¹² to 5 × 10⁻¹¹ cm³ molecule⁻¹ s⁻¹. Nevertheless, an activation energy of about 3 kcal mol⁻¹ can be derived via detailed balance from dissociation studies^{10,11} together with measurements of the equilibrium constant.^{7,8} These studies show that some uncertainties on the absolute value of the recombination rate constant of reaction 1, mainly on its temperature coefficient, still remain.

In addition, reaction 1,–1 has been recently found particularly suitable in studies of light-induced bistability,¹² stabilization of unstable states and oscillatory behavior,¹³ and chemical pulse wave.¹⁴ The interpretation of those investigations requires the detailed knowledge of the temporal evolution of the FSO₃ concentration due mainly to reaction 1,–1. Therefore, precise values of the rate constants for both forward and backward reactions are imperative.

The above-mentioned aspects emphasize the relevance of knowing more precisely the kinetics of the recombination–dissociation reaction in the F₂S₂O₆/FSO₃ system. Therefore, the present study was undertaken in order to clarify if the reaction is in its high-pressure limit for the mentioned studies, if this low rate of recombination is due to a barrier of activation, and in the case that no barrier exists, what are the reasons for such low value of the recombination rate constant. Another important question arises from the fact that special properties of the potential energy surface could be present and the general α/β parameter in the SACM calculations could still be in the standard range 0.46 ± 0.09. Therefore, if earlier reported low limiting high-pressure rate constants for this reaction are confirmed,⁹ this system may provide a stringent test for theoretical predictions of the SACM as emphasized in ref 2.

In this paper we report excimer laser flash photolysis/time-resolved absorption experiments of reaction 1,–1 over the temperature range 293–381 K and in the presence of He and CF₄ as bath gases, so that the approach to equilibrium is directly measured. In addition a detailed theoretical analysis of the results in terms of the canonical version of the statistical adiabatic channel model is also performed.

Experimental Section

The FSO₃ radicals were generated by 193-nm photolysis of F₂S₂O₆ using an ArF excimer laser (Lambda Physik EMG 101 MSC). After FSO₃ production, these radicals were monitored in real time by their visible absorption of light at 450 nm from a 250-W tungsten lamp powered by a dc supply. At this wavelength F₂S₂O₆ absorption is very weak.¹⁵ A cylindrical quartz vessel of 5 cm diameter and 5 cm length with flat optical windows, placed into a heavy aluminum envelope electrically heated, was employed as reaction cell. The laser photolysis beam with a cross section of 2.4 cm² (0.8 cm high and 3 cm wide) traversed the cell through the flat windows. Perpendicular to the laser beam the analysis light (0.3 cm high) runs across the laser-flashed volume, so that an optical path of 3 cm was probed close to the laser entrance window. The temperature of the reaction mixture was measured with a calibrated chromel–alumel thermocouple placed in contact with the wall of the cell close to the photolysis region. Room temperature experiments were also conducted in a rectangular aluminum cell with four flat quartz windows. The frontal section of this cell was slightly bigger than the cross section of the laser beam. Both sets of results were, within the error limits, in very good agreement. After passage through the reaction cell, the analytical beam was dispersed by a Zeiss MM12 monochromator and the light of the selected wavelength was detected by an RCA 1P28 photomultiplier coupled to a standard amplifying circuit¹⁶ and fed into a Nicolet 2090 digital oscilloscope triggered by the laser. The data resulting from single-shot experiments were stored on floppy disks and analyzed on a microcomputer. Eventually, the signals were displayed on a Houston X–Y recorder. The laser energy was measured by a Gentec pyroelectric detector. The gases were handled on a conventional vacuum system and the pressure was measured with a quartz spiral gauge. Typically, a static sample of 5 Torr of F₂S₂O₆ in the presence of 250–760 Torr of the diluent gases He or CF₄ was photolyzed at 193 nm at temperatures ranging from 293 to 381 K. After the addition of the third-body gas, ample time was allowed for diffusive mixing and for equilibrium to be established.

A Cary 14 spectrophotometer was employed for the absorption spectra measurement. A 10 cm long cylindrical quartz cell was enclosed in a Cary thermostable cell jacket. The temperature was adjusted to better than ±0.1 K by circulating water from a Haake thermostat through the cells jacket, and measured by a calibrated chromel–alumel thermocouple fitted to the wall of the cell. After constancy of the temperature was attained, sufficient time was allowed for equilibrium establishment. The absorbance of equilibrium mixtures of 70–90 Torr of F₂S₂O₆/FSO₃ in the range 310–334 K was measured at 450 nm with a spectral resolution of $\Delta\lambda(\text{fwhm}) = 0.4$ nm. The absorbance of each mixture was measured as a function of temperature. The results were reproducible with increasing and decreasing temperatures, according to previous studies that have shown that over wider pressure and temperature ranges the mixtures are stable in quartz vessels for long periods of time (many hours).⁸ At a given temperature, the attainment of equilibrium was indicated by the constancy of the absorbance readings. From the equilibrium constants given in ref 7 and 8, radical concentrations ranging from 1.6 × 10¹⁵ to 5.4 × 10¹⁵ molecules cm⁻³ were calculated as $[\text{FSO}_3] = (K_c[\text{F}_2\text{S}_2\text{O}_6])^{1/2}$. From this equation an uncertainty of less than 1% due to a temperature fluctuation of ±0.1 K is estimated.

F₂S₂O₆ was prepared by photolyzing a mixture of F₂ and SO₃ in a Pyrex reaction vessel with a Hanau Q700 mercury lamp. The F₂S₂O₆ was condensed at 195 K and small amounts of F₂SO₃ were eliminated by trap-to-trap distillations at 223 K.¹⁷ The purity grade of F₂S₂O₆ was verified by IR spectrophotometry. The diluent gases had the following stated purities: He 99.999%

(7) Dudley, F. B.; Cady, G. H. *J. Am. Chem. Soc.* **1963**, *65*, 3375.

(8) Castellano, E.; Gatti, R.; Sicre, J. E.; Schumacher, H. J. *Z. Phys. Chem. NF* **1964**, *42*, 174.

(9) San Román, E.; Aramendía, P. F.; Schumacher, H. J. *Anal. Asoc. Quim. Argentina* **1982**, *70*, 887. Aramendía, P. F. Doctoral Thesis, University of Buenos Aires, 1983.

(10) von Ellenrieder, G.; Castellano, E.; Schumacher, H. J. *Z. Phys. Chem. NF* **1968**, *57*, 19.

(11) von Ellenrieder, G.; Schumacher, H. J. *Z. Phys. Chem. NF* **1968**, *59*, 157.

(12) Zimmermann, E. C.; Ross, J. J. *Chem. Phys.* **1984**, *80*, 720.

(13) Zimmermann, E. C.; Schell, M.; Ross, J. J. *Chem. Phys.* **1984**, *81*, 1327.

(14) Kamer, J.; Reiter, J.; Ross, J. J. *Chem. Phys.* **1986**, *84*, 1492.

(15) King, G. W.; Santry, D. P.; Warren, C. H. *J. Mol. Spectrosc.* **1969**, *32*, 108.

(16) Porter, G.; West, M. A. In "Investigation of Rates and Mechanism of Reactions"; Part II, *Techniques of Chemistry*, 3rd ed.; Hammes, G. G., Ed.; Wiley: New York, 1974; Vol. VI.

(17) Gambaruto, M.; Sicre, J. E.; Schumacher, H. J. *J. Fluorine Chem.* **1975**, *5*, 175.

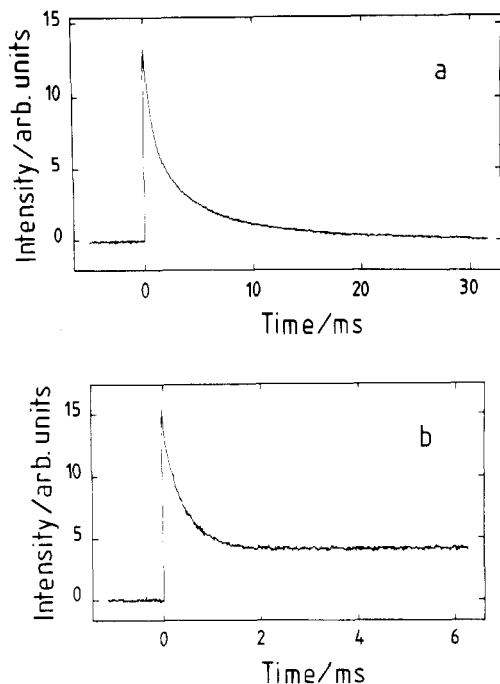


Figure 1. (a) Time dependence of the FSO_3 radical absorption at 450 nm, resulting from the 193-nm photolysis of a mixture of 5.9 Torr of $\text{F}_2\text{S}_2\text{O}_6$ and 560.1 Torr of CF_4 at 293 K. (b) Temporal profile of the FSO_3 radical absorption at 450 nm, following the photolysis of 4.8 Torr of $\text{F}_2\text{S}_2\text{O}_6$ and 694.8 Torr of CF_4 at 381 K.

(Union Carbide) and CF_4 99.7% (Matheson).

Results and Discussion

1. Data Analysis. Spectroscopic studies of the system (1,-1) show that the absorption spectra of $\text{F}_2\text{S}_2\text{O}_6$ and FSO_3 do not interfere.^{8,15} The $\text{F}_2\text{S}_2\text{O}_6$ presents a continuous absorption below 270 nm with increasing cross sections as the wavelength decreases. On the other hand, the FSO_3 radical has two weak diffuse systems in the near-infrared one at 1400–1300 nm and the other at 840–720 nm. In addition, there is a much stronger absorption between 550 and 380 nm.¹⁵ This absorption spectrum exhibits a well-resolved vibronic structure at the longer wavelength with origin at 516 nm (${}^2\text{E}(2) \rightarrow \bar{\text{X}}^2\text{A}_2$ transition). This structure disappears toward shorter wavelengths due to predissociation.

UV flash spectroscopy studies in this system have shown that FSO_3 radicals are produced predominantly.⁹ In this work, $\text{F}_2\text{S}_2\text{O}_6$ has been photolyzed with excimer laser radiation at 193 nm. At this wavelength a $\text{F}_2\text{S}_2\text{O}_6$ absorption cross section of $4.14 \times 10^{-18} \text{ cm}^2 \text{ molecule}^{-1}$ has been here measured. A quantum yield close to unity for photodissociation of the dimer ($\text{F}_2\text{S}_2\text{O}_6$) into two monomers (FSO_3 radicals) has been obtained by comparing the amount of initially produced radicals with the calculated number of photons absorbed.

The chemical relaxation has been observed by monitoring the concentration of the monomer using light absorption at 450 nm. At this wavelength FSO_3 absorption cross section is about 3 orders of magnitude larger than the one of $\text{F}_2\text{S}_2\text{O}_6$ (see below). Therefore, in the photolysis experiments the absorption of the dimer at this wavelength can be neglected.

Figure 1 shows typical transient absorption decay curves as detected in our experiments. At 450 nm the only light-absorbing species is the FSO_3 radical and, therefore, the absorption time profiles can be directly converted into FSO_3 concentration–time profiles provided the appropriate absorption cross section is known. The observed decays show a typical relaxation behavior into a chemical equilibrium. However, due to additional heating from the UV laser absorption there is a well-defined small increase in temperature in the reaction system. Therefore, the chemical relaxation is not back to the initial preflash equilibrium but to a new equilibrium at a somewhat higher temperature. A maximum increase in temperature of about 5 K has been detected in

the case of 250 Torr of He while the increase for 760 Torr of CF_4 is only about 1 K. At room temperature, this effect cannot be seen directly in our absorption profiles because the change in equilibrium concentration of FSO_3 is negligible (Figure 1a). However, at higher bath gas temperatures (Figure 1b) even an increase in temperature of about 1 K will induce measurable changes in the FSO_3 equilibrium concentration. The temperature dependence of the equilibrium constant $K_c = k_{-1}/k_1 = [\text{FSO}_3]^2/[\text{F}_2\text{S}_2\text{O}_6]$ is mainly determined by the dissociation rate constant k_{-1} . Since k_{-1} is very strongly dependent on temperature,^{10,11} the increase in temperature in the reaction cell has to be taken into account. It is calculated from the initially produced concentration of monomers and then added to the temperature measured before the laser pulse. Only about 15% of the energy of the photolysis photon ($148.0 \text{ kcal mol}^{-1}$) is used for dissociation. The rest will remain as excitation of the radicals. Because of the low rate of the chemical reaction, the relaxation of any excitation of the FSO_3 radicals in collisions with the heat bath is complete before any measurable quantity has recombined.

At 450 nm the measured FSO_3 absorbance–time profiles $A(t)$ are related to the concentration–time profiles by Beer–Lambert's law in the form

$$A(t) = -\ln [I(t)/I_0] = \sigma l [\text{FSO}_3] \quad (2)$$

$I(t)$ and I_0 are the transmitted and incident light intensities at time t , σ is the absorption cross section of the FSO_3 radical, l is the optical path length, and $[\text{FSO}_3]$ is the radical concentration at time t . The FSO_3 radical absorption cross section at 450 nm was determined from the spectrophotometric measurements. An absorbance vs $[\text{FSO}_3]$ plot was linear over the whole range of FSO_3 concentration. A cross section of $(4.2 \pm 0.37) \times 10^{-18} \text{ cm}^2 \text{ molecule}^{-1}$ was obtained from the slope of the Beer's law plot. Throughout this paper the error estimates quoted for our measurements represent two standard deviations. Similar results were found with lower spectral resolution, $\Delta\lambda(\text{fwhm}) = 3.3 \text{ nm}$, in the apparatus used for the time-resolved experiments. The temporal evolution of the radical concentration can be described by a simple kinetic equation

$$d[\text{FSO}_3]/dt = -2k_1[\text{FSO}_3]^2 + 2k_{-1}[\text{F}_2\text{S}_2\text{O}_6] \quad (3)$$

where k_1 and k_{-1} are the rate constants for recombination and dissociation, respectively, and $[\text{F}_2\text{S}_2\text{O}_6]$ is the concentration of the dimer. Equation 3 was numerically integrated by using a fourth-order Runge–Kutta algorithm with Gill coefficients.¹⁸ The best k_1 and k_{-1} values were obtained from a nonlinear least-squares fit of simulated FSO_3 decay curves to the experimental profiles.¹⁹ This procedure showed that, at room temperature, the temporal evolution of $[\text{FSO}_3]$ is determined by the first term in eq 3. Therefore, from those experiments only k_1 can be extracted. A preliminary value of $k_1 = 5.2 \times 10^{-14} \text{ cm}^3 \text{ molecule}^{-1} \text{ s}^{-1}$ at 293.2 K, together with k_{-1} extrapolated toward the temperature range of the present experiments,^{10,11} allows us to make an estimate of the relative importance of both terms in eq 3 as a function of temperature and, at a given temperature, along the decay profile. For instance, at 321.5 K and at 3 ms after the laser pulse, when about 50% of the FSO_3 radicals have been consumed, the rate of recombination is about 10 times larger than the rate of dissociation. However, recombination is only 2 times faster than dissociation at 10 ms. At the highest temperature, 381 K, the rate of recombination and the rate of dissociation differ in a factor of less than 2 along the whole decay profile. These factors show that, as temperature increases, an increasing contribution of the second term of eq 3 has to be expected. On the other hand, even at 321.5 K, the whole decay can only be fitted if both recombination and dissociation processes are taken into account. The numerical fitting procedure delivered k_1 at 293.2 K and a set of recombination and dissociation rate constants between 321.5 and

(18) Gill, S. *Proc. Cambridge Philos. Soc.* **1951**, *47*, 96.

(19) Pilling, M. J. In *Modern Gas Kinetics. Theory, Experiment and Application*; Pilling, M. J., Smith, I. W. M., Eds.; Blackwell: Boston, MA, 1987; pp 190–205.

TABLE I: Experimental High-Pressure Rate Constants and Equilibrium Constants for Reaction 1,-1

T/K	M	$k_{\text{rec},\infty}/\text{cm}^3 \text{ molecule}^{-1} \text{ s}^{-1}$	k_{∞}/s^{-1}	$K_c/\text{molecules cm}^{-3}$
293.2	CF ₄	$(4.52 \pm 0.58) \times 10^{-14}$		
293.4	He	$(4.77 \pm 0.51) \times 10^{-14}$		
321.5	CF ₄	$(4.78 \pm 0.56) \times 10^{-14}$	$(2.06 \pm 0.24) \times 10^{-1}$	$(4.31 \pm 0.17) \times 10^{12}$
333.9	CF ₄	$(4.81 \pm 0.61) \times 10^{-14}$	$(7.90 \pm 1.02) \times 10^{-1}$	$(1.64 \pm 0.18) \times 10^{13}$
356.0	CF ₄	$(5.16 \pm 0.53) \times 10^{-14}$	$(6.65 \pm 0.68) \times 10^0$	$(1.29 \pm 0.14) \times 10^{14}$
378.2	He	$(5.69 \pm 0.77) \times 10^{-14}$	$(3.65 \pm 0.49) \times 10^1$	$(6.41 \pm 0.19) \times 10^{14}$
381.0	CF ₄	$(5.51 \pm 0.98) \times 10^{-14}$	$(4.63 \pm 0.82) \times 10^1$	$(8.40 \pm 0.25) \times 10^{14}$

^a Reported values are averages of 8–16 experiments with total pressures ranging between 250 and 760 Torr.

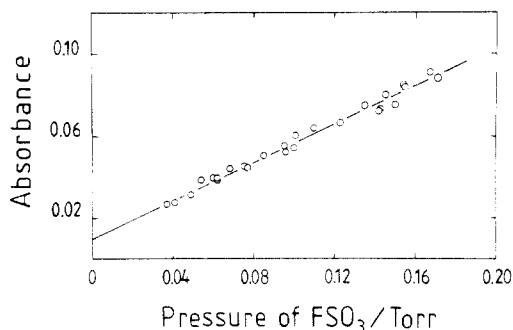


Figure 2. Pressure dependence of the absorbance of mixtures F₂S₂O₆/FSO₃ at 450 nm. The F₂S₂O₆ pressure ranged between 70 and 90 Torr and the temperatures between 310 and 334 K.

381 K. The equilibrium constants calculated agreed well with those extrapolated from the results of ref 7 and 8 obtained in the temperature range 423–523 K. However, the calculated FSO₃ concentrations which were used in the determination of the absorption cross section differed by about 15%. Therefore, a new absorption cross section of FSO₃ radical was obtained by plotting the absorbance of the equilibrium mixtures F₂S₂O₆/FSO₃ vs corrected FSO₃ radical concentrations (Figure 2). The slope of the straight line yields the new cross section of the FSO₃ radical while the intercept is due to a minor absorption of the F₂S₂O₆. In this way, $\sigma(\text{FSO}_3) = (3.64 \pm 0.32) \times 10^{-18} \text{ cm}^2 \text{ molecule}^{-1}$ and $\sigma(\text{F}_2\text{S}_2\text{O}_6) = (7.64 \pm 0.08) \times 10^{-22} \text{ cm}^2 \text{ molecule}^{-1}$ were derived at 450 nm. The relaxation profiles were analyzed again by using this cross section, and the final values of k_1 and k_{-1} changed by no more than 15%. A further adjustment of the FSO₃ cross section proved to be unnecessary. The experiments were analyzed at least up to 95% of the total decay. From these results we find that k_1 as well as k_{-1} are independent of the total pressure between 250 and 760 Torr and they also do not depend on the nature of the bath gas, even though the collision efficiency for CF₄ is typically 3 times higher than for He.^{20,21} These findings indicate that the reaction is certainly very close to the high-pressure regime, in agreement with studies of the thermal dissociation of F₂S₂O₆ where higher reactant concentrations were employed.^{10,11} Therefore, at each temperature only an average value of the rate constants $k_1 = k_{\text{rec},\infty}$, $k_{-1} = k_{\infty}$ and the ratio $K_c = k_{\infty}/k_{\text{rec},\infty}$ are given in Table I. Each value is an average of 8–16 measurements.

Over the temperature range 293–381 K the recombination data can be represented by the equation

$$k_{\text{rec},\infty} = 4.64 \times 10^{-14} (T/300)^{(0.72 \pm 0.25)} \text{ cm}^3 \text{ molecule}^{-1} \text{ s}^{-1} \quad (4)$$

while between 321.5 and 381 K the dissociation rate constant is given by

$$k_{\infty} = 2.09 \times 10^{14} \exp[-(11090 \pm 290)/T] \text{ s}^{-1} \quad (5)$$

The expression for the equilibrium constant in the range 321.5–381 K, obtained as the best fit of the individual k_{-1}/k_1 ratios, is as follows

$$K_c = 1.45 \times 10^{27} \exp[-(10730 \pm 380)/T] \text{ molecules cm}^{-3} \quad (6)$$

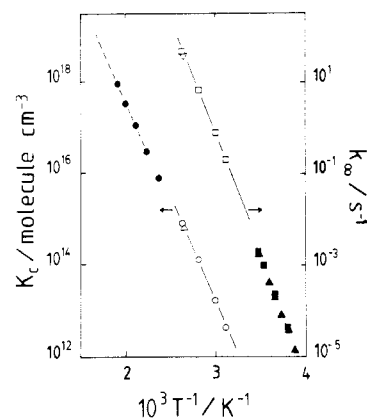


Figure 3. Comparison of the temperature dependence of k_{∞} and K_c values with previous determinations. k_{∞} values: \blacktriangle , ref 10; \blacksquare , ref 11; \square , this work (M = CF₄); ∇ , this work (M = He); —, eq 5. K_c values: \bullet , ref 8; ---, ref 7; \circ , this work (M = CF₄); Δ , this work (M = He); —, eq 6.

TABLE II: Comparison of ΔH°_{298} and ΔS°_{298} Values with Previous Data

method	$\Delta H^{\circ}_{298}/\text{kcal mol}^{-1}$	$\Delta S^{\circ}_{298}/\text{cal mol}^{-1} \text{ K}^{-1}$	ref
manometric	22.4	37.9	7
spectrophotometric	23.3		7
manometric	22.3 ± 0.3	37.6 ± 0.3	8
electron spin resonance	22.4 ± 0.9^a		24
laser flash photolysis	22.1 ± 0.7	38.2 ± 1.0	this work

^a In liquid phase.

The absolute value of the recombination rate constant is in very good agreement with previously reported values.^{9–11} The temperature dependence is consistent with an activation energy of $(0.5 \pm 0.2) \text{ kcal mol}^{-1}$ in good agreement with temperature-independent results.⁹ However, an activation energy of $3.0 \pm 0.6 \text{ kcal mol}^{-1}$ is evaluated via detailed balance with the results of ref 7, 8, 10, and 11. It is reasonable to assume a larger uncertainty in the temperature dependence calculated with the relationship $k_{\text{rec},\infty} = K_c k_{\infty}$ because the K_c and k_{∞} values are results of extrapolations. A comparison of the dissociation rate and equilibrium constants is shown in Figure 3. The straight lines represent the expressions from above, being least-squares fits to our data. Extrapolations of the k_{∞} and K_c values determined here toward the temperature ranges where previous data are available shows that the present results are somewhat higher than the earlier ones.

2. Standard Enthalpy and Entropy Changes of the Reaction. Reaction enthalpy $\Delta H^{\circ}_{354} = 22.0 \text{ kcal mol}^{-1}$ and entropy $\Delta S^{\circ}_{354} = 38.1 \text{ cal mol}^{-1} \text{ K}^{-1}$ changes at the mean temperature of 354 K for reaction 1,-1 are obtained from the temperature dependence of $K_p = K_c(RT)$. The extrapolation to 298 K is performed by calculating the changes in molar heat capacities, ΔC_p , from the vibrational frequencies of F₂S₂O₆²² and FSO₃.²³ Table II shows that our results agree very well with previous studies. The com-

(20) Troe, J. *J. Chem. Phys.* **1977**, *66*, 4745, 4758.

(21) Dove, J. E.; Hippler, H.; Troe, J. *J. Chem. Phys.* **1985**, *82*, 1907 and references therein.

(22) Qureshi, A. M.; Levchuk, L. E.; Aubke, F. *Can. J. Chem.* **1971**, *49*, 2544.

(23) Warren, C. H. *Chem. Phys. Lett.* **1979**, *68*, 407.

(24) Nutkowitz, P. M.; Vincow, G. *J. Am. Chem. Soc.* **1969**, *91*, 5956.

parison of the weak O–O linkage in $\text{F}_2\text{S}_2\text{O}_6$ with some other O–O-bond-containing fluorinated compounds presents some interest. A good approach to the O–O bond dissociation energy is provided by the thermal activation energy in the high-pressure limit. Larger values are reported for CF_3OOCF_3 ²⁵ (46.3 kcal mol⁻¹), SF_5OOSF_5 ²⁶ (37.2 kcal mol⁻¹), $\text{CF}_3\text{OOOCF}_3$ ²⁷ (30.4 kcal mol⁻¹), and $\text{SF}_5\text{OOOSF}_5$ ²⁸ (25.3 kcal mol⁻¹). It seems reasonable to attribute the small O–O bond energy in $\text{F}_2\text{S}_2\text{O}_6$ to the electron-withdrawing effect of the electronegative $\text{FS}(=\text{O})_2$ groups.

3. Extrapolation of the Limiting High-Pressure Recombination Rate Constants. Typical values of high-pressure recombination rate constants of radical–radical reactions (those reverse of simple bond fission reactions) range from nearly 1×10^{-12} to 5×10^{-11} cm³ molecule⁻¹ s⁻¹.^{29–31} However, the reported recombination rate constant, 4.5×10^{-14} cm³ molecule⁻¹ s⁻¹, is a factor of 18 below the lowest limiting high-pressure rate constant reported so far.⁵ Therefore, it seems adequate to check how far our experimental data are from the theoretically predicted high-pressure limit. For this purpose, a falloff curve which fits the experimental room temperature recombination rate constant has to be constructed. In order to do this, the limiting low-pressure recombination rate constant $k_{\text{rec},0}$ was calculated by means of the factorized formalism proposed by Troe.²⁰ Already reported values of the vibrational frequencies^{22,23} and rotational constants³² for the FSO_3 radical were employed. The evaluation of the $\text{F}_2\text{S}_2\text{O}_6$ rotational constants was done assuming a structure composed essentially of two FSO_3 moieties, identical with the FSO_3 radical. The two units are separated by a typical O–O bond distance and oriented with a dihedral angle of 107°. The resulting strong collision low-pressure rate constant was combined with a typical value of the collision efficiency $\beta_c = 0.5$ for CF_4 ^{20,21} to predict $k_{\text{rec},0} = [\text{CF}_4] \times 2.0 \times 10^{-30}$ cm³ molecule⁻¹ s⁻¹ at 293 K. This value is similar to the low-pressure rate constant for N_2O_5 recombination.⁶ Using this value, a fit of the falloff curve³⁴ through our experimental points in the range between 250 and 760 Torr was consistent with a limiting high-pressure rate constant of $(5.9 \pm 1.4) \times 10^{-14}$ cm³ molecule⁻¹ s⁻¹ close to our value of $(4.52 \pm 0.58) \times 10^{-14}$ cm³ molecule⁻¹ s⁻¹. The error limits take into account an uncertainty of ± 0.2 units in β_c and a factor of 3 in the calculated strong collision low-pressure rate constants. The center of the falloff curve $[\text{CF}_4]_c = k_{\text{rec},\infty}/k_{\text{rec},0}$ is expected to be around 1 Torr in this case, while this ratio is approximately equal to 23 Torr for the system N_2O_5 .⁶ This fact already indicates that at pressures around 1 atm the experimental rate constant is very close to the theoretical high-pressure limit. The observed independence of $k_{\text{rec},\infty}$ on the nature of the bath gas in the pressure range between 250 and 760 Torr supports this conclusion.

4. Theoretical Analysis of the Limiting High-Pressure Rate Constants. (i) *SACM Calculations.* It appears important at this stage to try to understand which is the origin of such small measured $k_{\text{rec},\infty}$ values. The lack of an appreciable temperature dependence of $k_{\text{rec},\infty}$ rules out the existence of an electronic energy barrier. Special characteristics of the potential energy surface could cause the apparently anomalous $k_{\text{rec},\infty}$ values for this reaction. The canonical version of the statistical adiabatic channel model¹ provides an useful method to determine limiting high-pressure rate constants. In addition, the essential molecular and potential energy surface features affecting these rate constants can be studied. The

application of this model requires the knowledge of the attractive interfragment potential and the relevant angular parts of the potential energy surface of the reaction. A SACM calculation performed for the reaction $\text{H} + \text{CH}_3 \rightarrow \text{CH}_4$ has been recently compared with quasi-classical trajectory and variational transition-state theory calculations using the same ab initio surfaces.³⁵ A very good agreement was found in all cases. Unfortunately, no information about the potential energy surface of reaction 1 is available. Therefore, a simple potential model, originally proposed by Quack and Troe,³⁶ has been employed in the present calculations. In this way, the variation of the electronic energy along the reaction coordinate (O–O elongation) is described by means of a Morse potential with a parameter $\beta = 3.5 \text{ \AA}^{-1}$, as calculated by using the stretching force constant of the O–O bond in H_2O_2 .³⁷ This approach seems to be justified by recent ab initio calculations showing that such force constants in H_2O_2 and in peroxytrifluoroacetic acid, $\text{CF}_3\text{C}(=\text{O})\text{O}-\text{OH}$, are essentially the same.³⁸ The limiting high-pressure rate constants for the recombination are calculated via detailed balance from those for the dissociation process. The $\text{F}_2\text{S}_2\text{O}_6$ frequencies, ν_i , that undergo the major attenuation along the reaction path during the dissociation process are given by $\nu_i = \nu_{i,e} \exp[-\alpha(r - r_e)]$, r being the interfragment distance. The analytical expression for $k_{\text{rec},\infty}$ in the factorized form, is^{1,2,35}

$$k_{\text{rec},\infty} = f_{\text{rigid}} k_{\text{rec},\infty}(\text{PSL}) \quad (7)$$

where $k_{\text{rec},\infty}(\text{PSL})$, the phase space limiting high-pressure rate constant, can be calculated when a totally loose transition state occurs. Therefore, f_{rigid} can be interpreted as a steric hindrance factor that reflects the fact that, at the critical separation, not all angular orientations of the radicals are possible. In terms of the transition-state theory, the value of f_{rigid} is an indication of the tightness of the transition state. $k_{\text{rec},\infty}(\text{PSL})$ depends strongly on the range of the interfragment potential. Since a detailed analysis of the model is given in ref 1, 2, and 35, in the present discussion we are only dealing with the relevant aspects of f_{rigid} . For this reaction the analytical factors in eq 7 are

$$k_{\text{rec},\infty}(\text{PSL}) = \frac{kT}{4h} \left(\frac{h^2}{2\pi\mu kT} \right)^{3/2} Q_{\text{cent}}^*(\text{PSL}) \quad (8)$$

where μ denotes the reduced mass of the reaction partners and $Q_{\text{cent}}^*(\text{PSL})$ the phase space limit centrifugal pseudopartition function. It is certainly convenient to factorize f_{rigid} as follows

$$f_{\text{rigid}} = A f_{\text{trans}} \quad (9)$$

where A is given by

$$A = \frac{9\pi^2 Q_{\text{cent}}^* F_{\text{AM}}^* Q_{\text{j}}}{32\sigma^* Q_{\text{cent}}^*(\text{PSL}) Q_{\text{vibrot}}^2} \exp\left(-\frac{\Delta E_{0Z}^*}{kT}\right) \quad (10)$$

Here, Q_{cent}^* denotes the centrifugal pseudopartition function, F_{AM}^* an angular momentum coupling correction factor, σ^* the effective symmetry number, Q_{vibrot} the rovibrational partition function of the FSO_3 radical, and ΔE_{0Z}^* is the adiabatic zero-point barrier of the lowest reaction channel. The quantities denoted by * depend on the α and β parameters. On the other hand, f_{trans} describes the contribution of the transitional modes, which change during the recombination from free rotors via hindered rotors into vibrations. This factor is defined by

$$f_{\text{trans}} = \frac{\prod_6 Q_{\text{m}}^*}{\prod_6 Q_{\text{m}}^*(\text{PSL})} \quad (11)$$

(25) Czarnowski, J.; Schumacher, H. J. *Z. Phys. Chem. NF* **1974**, *92*, 329.

(26) Czarnowski, J.; Schumacher, H. J. *Int. J. Chem. Kinet.* **1978**, *10*, 111.

(27) Czarnowski, J.; Schumacher, H. J. *Int. J. Chem. Kinet.* **1981**, *13*, 639.

(28) Czarnowski, J.; Schumacher, H. J. *Int. J. Chem. Kinet.* **1979**, *11*, 1089.

(29) Kerr, J. A.; Moss, S. J. *CRC Handbook of Bimolecular and Ter-molecular Gas Reactions*; CRC Press: Boca Raton, FL, 1981; Vol. II.

(30) Baulch, D. L.; Cox, R. A.; Hampson, R. F.; Kerr, J. A.; Troe, J.; Watson, R. T. *J. Phys. Chem. Ref. Data* **1984**, *13*, 1259.

(31) DeMore, W. B.; Margitan, J. J.; Molina, M. J.; Watson, R. T.; Hampson, R. F.; Kurylo, M. J.; Howard, C. J.; Ravishankara, A. R. *Chemical Kinetics and Photochemical Data for Use in Stratospheric Modelling*; Evaluation No. 7, 1985, JPL Publication 85-37.

(32) King, G. W.; Warren, C. H. *J. Mol. Spectrosc.* **1969**, *32*, 138.

(33) Harvey, R. B.; Bauer, S. H. *J. Am. Chem. Soc.* **1954**, *76*, 859.

(34) Troe, J. *J. Phys. Chem.* **1979**, *83*, 114.

(35) Cobos, C. J. *J. Chem. Phys.* **1986**, *85*, 5644. Cobos, C. J. *Int. J. Chem. Kinet.*, in press.

(36) Quack, M.; Troe, J. *Ber. Bunsen-Ges. Phys. Chem.* **1974**, *78*, 240.

(37) Uzer, T.; Hynes, J. T.; Reinhard, W. P. *Chem. Phys. Lett.* **1985**, *117*, 600.

(38) Politzer, P.; Bar-Adon, R.; Miller, R. S. *J. Phys. Chem.* **1987**, *91*, 3191.

TABLE III: Comparison of Calculated and Experimental Rate Constants of Reaction 1 in the Limit of High Pressures^a

T/K	A/10 ⁻¹	f _{trans} /10 ⁻⁴	f _{rigid} /10 ⁻⁴	k _{rec,∞} /10 ⁻¹⁴ cm ³ molecule ⁻¹ s ⁻¹		
				phase space limit ^a (α/β → ∞)	SACM (α/β = 0.46)	exptl
293.2	3.90	8.34	3.25	13 900	4.52	(4.52 ± 0.58)
321.5	3.95	8.16	3.22	14 400	4.64	(4.78 ± 0.56)
333.9	3.97	8.04	3.19	14 600	4.66	(4.81 ± 0.61)
356.0	4.00	7.90	3.16	14 900	4.71	(5.16 ± 0.53)
381.0	4.03	7.70	3.10	15 300	4.74	(5.51 ± 0.98)

^a Calculated with eq 8.

where Q_m^* are the pseudopartition functions of five transitional modes and the external rotation with quantum number κ . For reaction 1 these five modes correspond to the deformation oscillators which appear along the reaction path. Since all the channel eigenvalues are much smaller than kT , classical partition functions can be employed in eq 11. Then

$$f_{\text{trans}} \approx \left[\frac{\Gamma(1 + \chi_m)}{\Gamma(3/2)} (kT)^{\chi_m - 1/2} \right]^5 \times \frac{\prod_6 B_i^{1/2}}{[B_1 + (C - B_1)\gamma]^{1/2} \prod_5 [B_i + (\nu_i - B_i)\gamma]^{\chi_m}} \quad (12)$$

In this equation, Γ denotes the gamma function, B_i are the FSO₃ rotational constants, B_1 is one of the smallest B_i , and C is the highest F₂S₂O₆ rotational constant. The relevant deformation frequencies ν_i are correlated to the B_i in the order of increasing energy. Finally, γ and χ_m , which are sensitive functions of the ratio α/β ,¹ play an important role in the calculation of $k_{\text{rec},\infty}$. When $\alpha/\beta \rightarrow \infty$ the phase space limit is reached, $f_{\text{rigid}} = 1$ and $k_{\text{rec},\infty} = k_{\text{rec},\infty}(\text{PSL})$. On the other hand, $k_{\text{rec},\infty}$ decreases when the ratio α/β decreases. The $k_{\text{rec},\infty}$ value measured at 293.2 K was fitted with eq 7–12 by employing $\alpha/\beta = 0.46$. By means of this value the temperature dependence of $k_{\text{rec},\infty}$ was theoretically predicted. The results are shown in Table III. Within the error limits, the agreement between experimental and theoretical results is very good. It is interesting to note that the ratio α/β used in the fit is in excellent agreement with the average value 0.46 ± 0.09 found for an extensive number of recombination–dissociation reactions.² The $k_{\text{rec},\infty}(\text{PSL})$ listed in Table III are similar to those calculated for many other reactions,² showing that the low experimental $k_{\text{rec},\infty}$ values are mainly due to the small f_{rigid} . The factor $f_{\text{rigid}} = 3.2 \times 10^{-4}$ obtained for this reaction is noticeably smaller than for other recombinations, ranging between 2.0×10^{-3} (for NO₂ + NO₂^{2,5}) and almost 1 (for Cl + NO₂). As seen in eq 10–12, f_{rigid} depends on the rotational constants B_i . The smaller the B_i values are, the smaller are the f_{rigid} values. Therefore, if any special feature of the potential energy surface can be discarded, the small f_{rigid} value could be mainly attributed to the magnitude of B_i . This value of f_{rigid} indicates that this reaction occurs through a tight transition state. In this case, the SACM predicts an average critical elongation of 3.2 Å at room temperature. Even though this bond length is appreciably large, the calculations show that the motions of the fragments are strongly restricted by angular forces arising from the degrees of freedom orthogonal to the reaction coordinate. This fact produces a contraction of the available phase space consistent with a very tight transition state. The simple potential employed precludes a reliable evaluation of the angular conformation of the transition state.

(ii) *Influence of the Potential Parameters on the Limiting High-Pressure Rate Constants.* Due to the lack of knowledge

of the real potential, we have also studied the influence of angular and radical potentials on SACM calculations of $k_{\text{rec},\infty}$. For this, the relevant potential parameters α and β were systematically changed, provided the room temperature $k_{\text{rec},\infty}$ value was fitted. In these conditions, when β was varied between 2.5 and 4.4 Å⁻¹, a relationship $\alpha/\beta = 0.49 - 0.12/\beta$ resulted, which has the same form for other reactions.^{39,40} This means that a reasonable change in the range of the radical potential does not affect significantly the ratio α/β . Recent ab initio calculations⁴¹ support the approximate constancy of the ratio α/β found in ref 2. On the other hand, such a change in β causes a variation in f_{rigid} of only about 18%, which does not account for the very low f_{rigid} found for this reaction. It is interesting to note that, for the simplest peroxide H₂O₂, experimental specific rate constants, product quantum state energy distributions, and the limiting high-pressure recombination rate constant can be correctly described by SACM calculations.⁴² These features can be reproduced by using either the simplified version of the microcanonical model⁴³ with $\alpha/\beta = 0.44$ or the detailed model³⁶ employing $\alpha/\beta = 0.50$. The range parameter α/β in the case of H₂O₂ is very close to our value for the more complex peroxide F₂S₂O₆. For the H₂O₂ recombination the $k_{\text{rec},\infty}$ value of 1.5×10^{-11} cm³ molecule⁻¹ s⁻¹ is about a factor of 300 larger than for the F₂S₂O₆ recombination. Since a similar $k_{\text{rec},\infty}(\text{PSL})$ is calculated for both reactions, f_{rigid} comes out to be responsible for such difference in the high pressure rate constants.

Summary

The present paper reports direct determinations of absolute rate constants for reaction 1,–1 in the high-pressure limit over the temperature range 293–381 K. The thermochemical parameters of the system ΔH°_{298} and ΔS°_{298} were also obtained from the experimentally derived equilibrium constants. The measured $k_{\text{rec},\infty}$ values are noticeably smaller than the frequently claimed normal. A SACM calculation reproduces the small experimental $k_{\text{rec},\infty}$ value if a standard α/β ratio is employed.

Acknowledgment. This research project is supported by the Consejo Nacional de Investigaciones Científicas y Técnicas and the Comisión de Investigaciones Científicas de la Provincia de Buenos Aires. Part of the equipment used in the present work was provided through the Cooperation Agreement between the University of Mainz (W. Germany) and the University of La Plata (Argentina). We also thank the Stiftung Volkswagenwerk for a partnership project with Professor J. Troe.

Registry No. FSO₃, 21549-02-0.

(39) Cobos, C. J.; Troe, J. *Chem. Phys. Lett.* **1985**, *113*, 419.

(40) Cobos, C. J. *Int. J. Chem. Kinet.* **1986**, *18*, 459.

(41) Wolf, R. T.; Bathia, D. S.; Hase, W. L. *Chem. Phys. Lett.* **1986**, *132*, 493.

(42) Brouwer, L.; Cobos, C. J.; Troe, J.; Dübal, H. R.; Crim, F. F. *J. Chem. Phys.* **1987**, *86*, 6171.

(43) Troe, J. *J. Chem. Phys.* **1983**, *79*, 6017.